Advanced Photonics Research

ADVANCED PHOTONICS RESEARCH Open Access

www.adpr-journal.com

RESEARCH ARTICLE OPEN ACCESS

Surface Plasmon Resonance-based Biosensing Towards the Detection of Multidrug-Resistant Tuberculosis

Sipho H. Chauke[1,2] | Lerato Hlekelele[3] | Charles Maphanga[1] | Mabotse Tjale[1] | Felix S. Dube[2] | Saturnin Ombinda-Lemboumba[1,4] | Patience Mthunzi-Kufa[5]

[1]Biophotonics, Photonic Centre, Manufacturing, Council for Scientific and Industrial Research (CSIR), Pretoria, South Africa | [2]Department of Molecular and Cell Biology, University of Cape Town, Cape Town, South Africa | [3]Centre for Nanostructures and Advanced Materials, DSI-CSIR Nanotechnology Innovation Centre, Council for Scientific and Industrial Research (CSIR), Pretoria, South Africa | [4]Departement de Physique, Université des Sciences et Techniques de Masuku, Franceville, Gabon | [5]School of Science, College of Science, Engineering and Technology, University of South Africa, Florida, South Africa

Correspondence: Sipho H. Chauke (schauke@csir.co.za)

Received: 14 August 2025 | **Revised:** 10 December 2025 | **Accepted:** 14 January 2026

Keywords: bioconjugation | detection | DNA hybridization | genes | multi-drug-resistant tuberculosis | mutations | nanoparticles | surface plasmon resonance

ABSTRACT

Current diagnostic tools for multidrug-resistant tuberculosis (MDR-TB) are molecular assay-based and have challenges associated with labor-intensive workflows, complex laboratory infrastructures, and limited mutation coverage. This highlights the need for alternative techniques that can be used as diagnostic tools for MDR-TB. In this study, we demonstrated the use of an surface plasmon resonance (SPR)-based biosensor chip for the detection of selected genes (*InhA*, *KatG*, and *RpoB*) within the MDR-TB genome using single-stranded deoxyribonucleic acids (ssDNA) targets and thiolated probes. The probes were successfully functionalized to AuNPs and confirmed using UV–vis and DLS. On SPR-based detection, the hybridization of the selected probes to complementary and non-complementary targets induced changes in the resonance angles. The hybridization of the selected probes to the targets was observed at resonance angles of 46.85, 46.77, 45.84, and 46.91° for *the IS6110*, *InhA*, *KatG*, and *RpoB* genes, respectively. In contrast, the unhybridized probe and the non-complementary targets exhibited resonance angles of 46.33, 46.05, 45.53, and 45.85° for *the IS6110*, *InhA*, *KatG*, and *RpoB* genes, respectively. The data showed that SPR-based biosensing can be refined and considered as an alternative approach to detect and differentiate between different ssDNA targets using thiolated probes as biorecognition elements for MDR-TB detection.

1 | Introduction

Tuberculosis (TB) remains one of the most prevalent and fatal communicable diseases caused by a bacterium [1, 2]. According to the World Health Organization (WHO) 2024 Global TB report, TB caused 2.7 million infections and 1.25 million deaths worldwide [3]. In South Africa, ≈270,000 people were infected with TB, of which 13,000 contracted different forms of drug-resistant TB [3]. Furthermore, 56,000 people in South Africa died due to TB infections, with 31,000 deaths attributed to people living with human immunodeficiency virus [3].

Although TB is curable with first-line drugs, rifampicin (RIF), isoniazid (INH), ethambutol (EMB), and pyrazinamide (PZA), other factors such as inappropriate antibiotic use, poor patient adherence to treatment, and the overprescription of incorrect therapies can contribute to the significant rise in drug-resistant strains of TB [2–4].

In 2023, only 2 in 5 people diagnosed with TB had access to drug-resistant TB treatment worldwide [3]. This limited access complicates TB treatment management, as drug-resistant TB requires complex drug regimens and extended treatment periods [5, 6]. Therefore, the diagnosis and identification of drug resistance

are essential to reduce the high mortality and morbidity associated with drug-resistant TB [3, 6, 7]. There is therefore a need for alternative, rapid, and sensitive diagnostic tools that can identify drug-resistant TB mutations, ensuring timely and appropriate treatment administration to prevent the transmission and progression of severe cases.

Current diagnostic tools for drug-resistant TB detection include assays such as the Xpert MTB/RIF*plus*, Genoscholar NTM + MDRTB II, GenoType MTBDR*plus*, and drug susceptibility tests such as genotypic and phenotypic drug susceptibility testing (gDST and pDST) [5, 8]. These diagnostic tools target the detection of canonical mutations within gene targets for the two first-line drugs, *RpoB* for RIF resistance and *InhA* and *KatG* for INH resistance [9–12]. More specifically, they target gene loci commonly prone to mutations, such as mutations in loci 459, 511, 526, and 531 for *RpoB*, 241, 315, and 289 for *KatG*, and 15 for *InhA* [13, 14].

Although the current diagnostic tools are effective in diagnosing drug-resistant TB, they have limitations, such as limited mutation coverage, being laboratory-based, and requiring established infrastructures [5, 8, 15, 16]. Additionally, these diagnostic tools require regular maintenance, which limits their capabilities as diagnostic tools for resource-limited settings [15, 16]. Efforts to find alternative sensitive methods and/or point-of-care biosensors for detecting and diagnosing TB and multidrug-resistant (MDR)-TB have led to the evaluation of alternative label-free and rapid assays, such as optical- and immunosensor-based techniques [17–19]. One optical-based technique that has shown high sensitivity for the detection of proteins, deoxyribonucleic acids (DNA), and other small molecules is surface plasmon resonance (SPR) [18]. It is based on the excitation of surface plasmons on the metal-dielectric interface on the surface of the sensor chip [20–23]. Moreover, these surface plasmons are extremely sensitive to any alterations made on the sensor surface [20, 23]. Alterations influence changes in the signal, which, in turn, can be interpreted as changes in the reflected or transmitted intensity, refractive index, and/or resonance angle shifts [20, 23].

SPR offers distinct advantages over other sensing platforms (i.e., fluorescence-based assays), such as the detection of minor changes in the refractive index at very low analyte concentrations, its label-free nature that eliminates the need for fluorescent tags, and its simple experimental workflows that can reduce potential interferences [20–22, 24, 25]. Moreover, SPR is highly versatile by facilitating the real-time analysis of diverse molecular interactions, such as protein–protein, protein–DNA, and protein–ligand binding kinetics [25–28]. Moreover, its ability for portability and multiplexing are added advantages that the SPR platform offers [22, 24, 29–32].

Despite being a label-free detection technique, SPR-based platforms can be coupled with nanomaterials such as gold nanoparticles (AuNPs) to amplify the signal [22, 33–37]. Due to the characteristics of AuNPs and their ability to agglomerate, a characterization technique known as dynamic light scattering (DLS) can be used to determine the hydrodynamic diameter/size of the nanoparticles [38, 39]. In addition, the electrical potential difference, or surface net charge, also known as the zeta potential (ζ), on the surface of the nanoparticles can also be evaluated [38, 39]. Similarly, nanoparticles can be conjugated to the molecules of interest and analyzed for changes in their hydrodynamic size after bioconjugation [40]. These molecules of interest bind through different techniques such as covalent bonding, direct (absorption), or affinity binding [41–43]. Once bound, these molecules can be detected using various platforms, including SPR.

Several studies have evaluated the use of SPR for the detection of TB using antibodies such as MPT64 and Ag85 [44–46]. These studies demonstrated the sensitivity of an SPR-based biosensor with low quantities of 10 pg/mL [44–47]. For instance, in a study by Trzaskowski et al. in 2018 [46], a miniature, portable SPR sensor chip device was fabricated and used to detect *Mycobacterium tuberculosis* (MTB), using anti-Ag85 antibodies targeting the MPT64 protein. In addition, similar studies used an SPR-based biosensor chip to detect the *IS6110* complex and the *RpoB* gene within the MTB genome using oligonucleotides [45, 48–50].

While SPR has been evaluated for the detection of TB using antibodies and oligonucleotides targeting the *IS6110* complex and the *RpoB* gene, this study introduces a unique probe design specifically targeting MDR-TB single-nucleotide mutations in gene targets, *InhA*, *KatG*, and *RpoB*. This refinement distinctly addresses a critical need for higher mutation coverage and more effective detection methods for drug-resistant TB strains. Moreover, by assessing the hybridization of the probes targeting specific MDR-TB mutations, this study contributes to the advancement of TB and MDR-TB diagnostics, offering the detection of heteroresistance. In this study, the focus on MDR-TB mutations provides a significant addition to the existing literature, with the potential to revolutionize the field of TB diagnosis and treatment, which could enable healthcare professionals to identify drug-resistant mutations (including heteroresistance) quickly and accurately for effective disease management and improved diagnostic outcomes. To achieve this, we developed a simple and label-free SPR-based biosensor chip to detect MDR-TB genes and their associated mutations. The SPR setup and single-stranded (ss) DNA probes were utilized to recognize MDR-TB genes on the SPR-based biosensor chip. The ssDNA probes targeted the *IS6110* complex and first-line drug gene targets (*InhA*, *KatG*, and *RpoB*). Furthermore, the proposed method, SPR, was used to assess the hybridization of the probes with complementary and non-complementary target DNA. Based on the data collected in this study, we established the relationship between the hybridization/binding properties of the probe and the gene targets using UV-visible spectroscopy (UV–vis) and SPR.

2 | Materials and Methods

2.1 | DNA Probe Design and Synthesis of ssDNA

Specific ssDNA targets and probes were designed to target loci 511 for the *RpoB* gene, 291 for *KatG*, and 15 for *InhA*. The MTB H37Rv strain's nucleotide sequence was obtained from the National Center for Biotechnology Information (NCBI) (GenBank: AL123456.3) and used as a reference to introduce mutations to loci 511 (L511P), 291 (A291V), and 15 (M15T) for *RpoB*, *KatG*, and *InhA*, respectively. Specific thiolated probes were designed to target sequences within the genes of interest, as listed in Table 1. The probes and target sequences were designed using BioEdit V7.1 (https://bioedit.software.informer.com/7.1/). A non-complementary probe with less than 15% sequence

TABLE 1 | Sequences of thiolated ssDNA probes, complementary, and non-complementary targets for MDR-TB genes of interest, presented in the 5′ to 3′ orientation.

Name	Sequences (5′ – 3′)
Probes (complementary to the targets)	
IS6110 probe	TGAACCGGATCGATGTGTAC
InhA probe	AGATATAGCTCCCGTCCTCG
KatG probe	CGATGACGTGCAGCCGAAGT
RpoB probe	CGTACCGTCGTTTACCGGGC
Target DNA sequence	
IS6110	GTACACATCGATCCGGTTCA
InhA	CGAGGACGGGAGCTATATCT
KatG	ACTTCGGCTGCACGTCATCG
RpoB	GCCCGGTAAACGACGGTACG
Non-complementary	ACTCCTTCAACCGCTTCCAC

complementarity to the target sequences was used as a negative control. This sequence was intentionally selected to represent a stringent test for non-specific binding, thereby enabling a robust assessment of the assay's specificity for detecting TB- and MDR-TB–associated sequences.

2.2 | Nanoparticle Functionalization and Characterization

In this study, bioconjugation was performed by adding 100 µL of gold nanoparticles (AuNPs) (~90 nm) (CytoDiagnostics, Canada) into a 1.5 mL centrifuge tube. Stock solutions (100 µM) of the thiolated probes were diluted to concentrations of 1, 2.5, 5, 10, 25, 50, and 75 µM. These were mixed in a 1:2 ratio with the AuNPs in microcentrifuge tubes and then placed on an orbital shaker for 1 h. Subsequently, 100 µL of the AuNPs-probe solution was mixed with different concentrations (1, 2.5, 5, 10, 25, 50, 75, and 100 µM) of the complementary/non-complementary targets and incubated for 30 min on an orbital shaker. The samples were analyzed using UV–vis.

Subsequently, the hydrodynamic size and zeta potential of the bioconjugates (AuNPs-ssDNA) were analyzed using DLS. The hydrodynamic size and zeta potential of the AuNPs were measured before and after bioconjugation using a Zetasizer (LB-550, Horiba Ltd, Japan).

2.3 | Preparation of Biosensing Surface

2.3.1 | Coating the Glass Substrate with Gold

The glass slides (5 × 5 cm) were washed with absolute ethanol and rinsed with ultrapure water in a sonicating bath for 10 min each. The washed slides were dried under nitrogen (N_2) gas and coated with thin films of titanium (5 nm) and gold (50 nm) using a physical vapor deposition system (HEX deposition system, Korvus Technology; United Kingdom). The coated slides were air-dried and stored at room temperature in an air-tight container.

2.3.2 | Probe Immobilization

The Au-coated slides were washed with absolute ethanol, rinsed with ultrapure water, and dried under N_2 gas. The concentrations of the probe used in the SPR experiments were optimized through UV–vis (as described in Section 2.2). Thirty microliters of the thiolated probes (10 µM) (Table 1) were immobilized on the slides and incubated overnight in the dark at 4°C. Following incubation, the slides were washed with 1X Phosphate-buffered saline (PBS) (Thermofisher, South Africa) to remove any unbound probes. The slides were air-dried at room temperature, and 30 µL of the ssDNA targets (10 µM) were added to the slides and incubated for 30 min in the dark at 4°C. The slides were washed with ultrapure water, allowed to dry, then washed with 1X PBS (pH 7.2) to remove any unbound DNA. The slides were dried and analyzed using the SPR setup (Figure 1).

2.3.3 | The Optical Biosensing Setup

The custom-built SPR-based biosensing platform was assembled using a 632.8 nm Helium–Neon (HeNe) laser with 2.0 mW power (as described in our previous publication) [51]. The reflected light from the sensor chip and the prism was captured using a photodetector connected to a computer for signal processing, as shown in Figure 2.

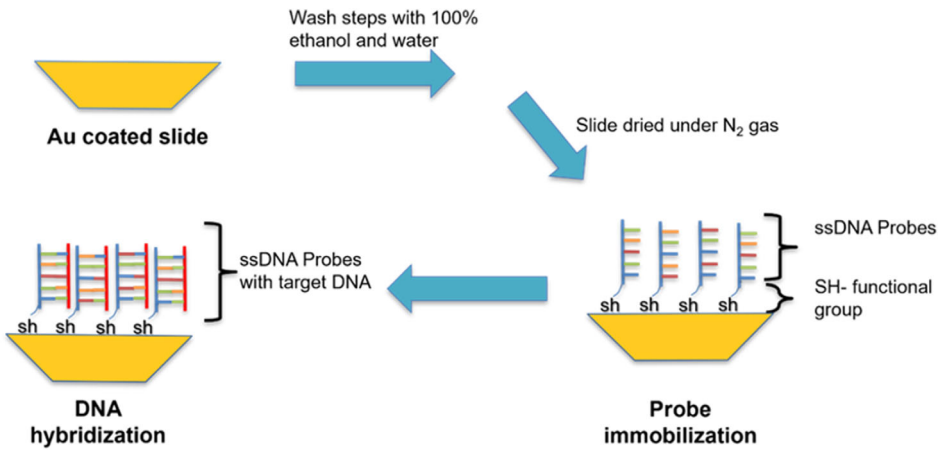

FIGURE 1 | A schematic diagram of probe immobilization and DNA hybridization, including washing steps of the sensor chip.

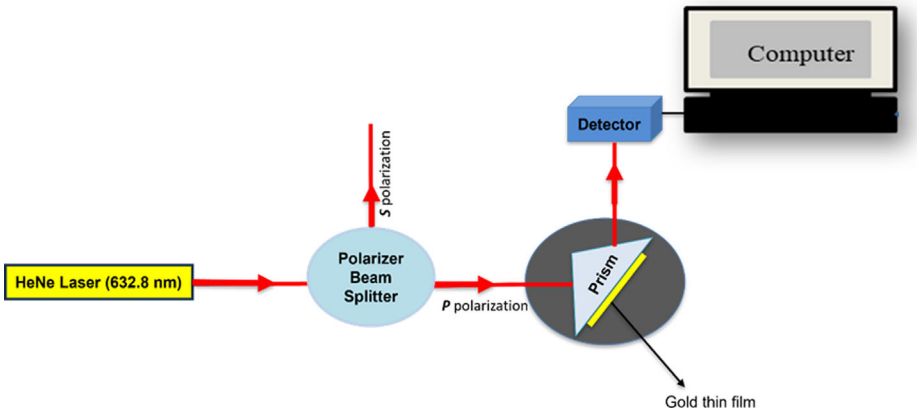

FIGURE 2 | An illustration of the SPR setup used in this study. The setup shows a HeNe laser beam passing through a polarizing beam splitter, with the *p* polarization of light being reflected from the BK7 glass prism with a biosensor chip on it [51].

The biosensing platform was optimized for its signal-to-noise ratio through optimized optical alignment, the use of a stable light source, and integrated references to enhance the detection of slight changes in the resonance and incident angles.

2.3.4 | The Detection Limits of the Optical Setup

The limit of detection (LOD) and limit of quantitation (LOQ) of the SPR platform for each probe were determined using the thiolated probes at different concentrations of 1, 5, 10, 50, and 100 μM. The probes were immobilized on the sensor chip as described in Section 2.3.2 and analyzed using the optical biosensing setup.

2.4 | Statistical Analysis

All statistical analyses were performed using OriginPro 8 software. The repeatability of each SPR experiment for each gene (in three independent experiments, $n = 3$) was determined using equation (1), while the LOD and LOQ of the SPR platform for each probe were quantified using Equations (2) and (3) [52], respectively.

$$\text{Repeatability} = \frac{\text{Resonance angle shift mean}}{\text{Resonance angle shift mean} + \text{Standard error}} \times 100 \quad (1)$$

$$\text{LOD} = 3.3 \times \frac{\sigma}{S} \quad (2)$$

$$\text{LOQ} = 10 \times \frac{\sigma}{S} \quad (3)$$

where σ is the standard deviation of the reference measurements and S the slope of the calibration curve of each response.

In addition, hybridization signal differences between the complementary and non-complementary targets were evaluated using a Tukey's honest significant difference (HSD) test (coupled with Levene's test for variance homogeneity) for pairwise comparisons. Independent experimental replicates ($n = 3$) were averaged, and the statistical significance was defined as $p < 0.05$, with a 95% confidence interval.

3 | Results and Discussion

3.1 | UV–Visible Spectroscopy

UV–vis is known for its ability to quantify the purity and concentration of a sample [53]. In this study, UV–vis was used to assess the changes in the absorption intensity with the addition of the probe and targets (complementary and non-complementary) to the AuNPs. The results of the different concentrations of the probe conjugated to the AuNPs obtained using UV–vis are presented in Figure 3. At a wavelength of 570 nm, the AuNPs exhibited a strong absorption peak, and thus, the effects of changing the concentrations of the probes bound to the AuNPs were evaluated. Subsequently, the bioconjugates' absorption at 570 nm was used to establish the intensity's linearity as a function of increasing probe concentration (Figure 3).

Across all genes, at a wavelength of 570 nm, as the concentration of the added ssDNA probes increased, there was a decrease in the absorption intensity (Figure 3). The decrease in the absorption

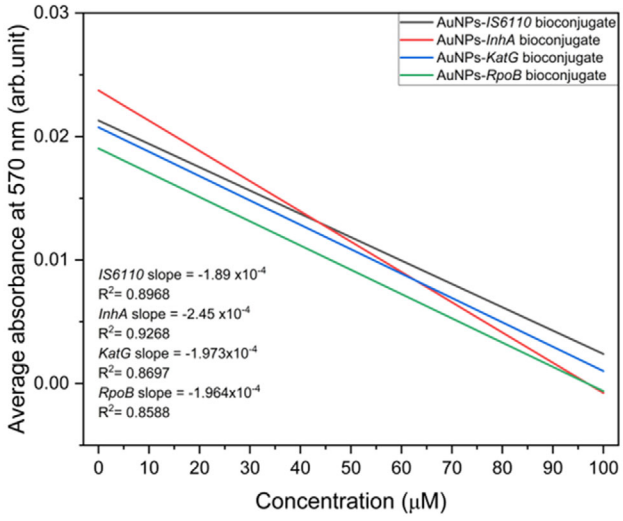

FIGURE 3 | The linearity and saturation behavior of ssDNA probes bound to AuNPs at different concentrations represented by the average absorption intensity at 570 nm (sample absorbance minus reference AuNP absorbance), plotted against DNA concentration (1 to 100 μM concentrations).

intensity, as the concentration increased, suggests the attachment of probes onto the AuNPs, thus producing low absorption intensities of the bioconjugates. Similar findings were noted in a study conducted by McCarte et al. in 2022 [54].

For each gene, the AuNPs' reference data were subtracted from the observed absorbance at different concentrations and plotted against the DNA concentration (at 570 nm), as shown in Figure 3. The function of each gene showed a linear response with gradients or slopes of -1.89×10^{-4}, -2.45×10^{-4}, -1.973×10^{-4}, and -1.964×10^{-4} for genes *IS6110*, *InhA*, *KatG*, and *RpoB*, respectively. When considering the linear regression equation, in this study, the gradients or slopes indicated the average change in the absorption intensity with increasing probe concentration.

Moreover, the R^2 values for *IS6110*, *InhA*, *KatG*, and *RpoB* genes were 0.8968, 0.9268, 0.8697, and 0.8588, respectively (Figure 3). Moreover, since the R^2 values (the coefficient of determination) were slightly closer to 1, this indicates that a greater proportion of the variation in the observed sample data was less likely due to residual variation (errors).

As shown in Figure 4a–d, the observed absorption intensity of the AuNPs decreased with the addition of the probes, complementary, and non-complementary targets. Moreover, the conjugation of the ssDNA probes to the AuNPs, which was enabled by the thiol groups on the probes, had high binding affinities to the AuNPs [55]. This is because of the conferred covalent bond formed between the probe and the AuNPs [56, 57]. This extended coverage stabilized the colloidal dispersion and altered the local refractive index surrounding the AuNPs, thereby reducing their SPR intensity and overall absorption of light by the AuNPs at 570 nm [57, 58]. In a similar study by Zhang et al. in 2018 [59], they also noted that an increase in oligo concentration led to a decrease in the absorption of intensity. Furthermore, the decrease in the absorption intensity of the bioconjugate bound to the complementary DNA was due to DNA hybridization, thus resulting in less light being absorbed by the AuNPs [60]. The decreased absorption intensity observed for the *InhA gene* (in Figure 4b), in the presence of the non-complementary target, could be attributed to different binding conformations on the AuNPs [61]. Overall, the observed decrease in the absorption intensity across all probe concentrations and targets reflects both

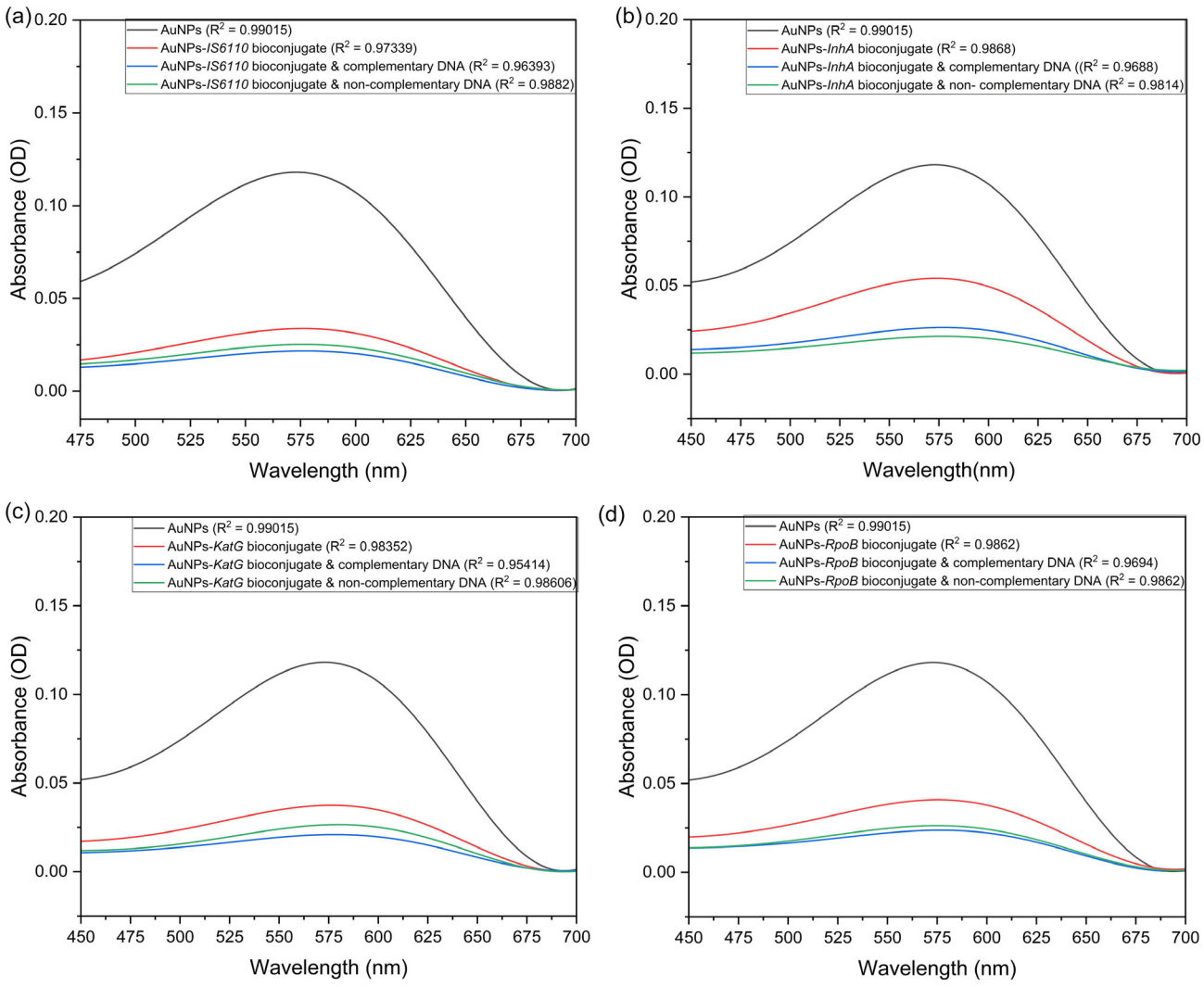

FIGURE 4 | UV–vis spectra showing mean hybridization responses of thiolated probes (10 μM) bound to AuNPs at 570 nm. The spectra illustrate changes in the absorption intensity upon the addition of complementary and non-complementary DNA to the AuNP–probe bioconjugates for gene targets (a) *IS6110*, (b) *InhA*, (c) *KatG*, and (d) *RpoB*.

surface modification and the stabilization effects that suppressed nanoparticle aggregation and plasmonic interactions.

3.2 | Characterization of Gold Nanoparticles using DLS

The quantification of the core size, conjugated molecules, and surface shell of a nanoparticle in a liquid is referred to as the hydrodynamic size [62, 63]. Furthermore, a particle's hydrodynamic size increases with the addition of biomolecules on the particle's surface [62]. In this study, the use of DLS enabled the determination of the nanoparticle distribution and aggregation, which could not be distinguished using UV–vis. Further evidence of the bioconjugation/binding of the ssDNA probes to the AuNPs was therefore assessed using DLS.

According to the manufacturer's specifications, the hydrodynamic size of each gold nanoparticle was reported as 93 nm. However, the DLS size distribution profile indicated that the hydrodynamic size of the particles was 89.72 nm (Figure 5). These slight changes in the hydrodynamic size could have been influenced by fluctuations in the temperature during analysis [64].

In addition, the hydrodynamic size distribution of the nanoparticles conjugated to the probes indicated an increase in the hydrodynamic size when compared to the untreated/bare nanoparticles (Figure 5). The average hydrodynamic sizes (in nm; ± SEM) noted for the AuNPs, *IS6110*, *InhA*, *KatG*, and *RpoB* bioconjugates were 89.72 nm ± 4.486, 241.45 nm ± 12.073, 349.6 nm ± 17.479, 205.8 nm ± 10.291, and 200.5 nm ± 10.025, respectively (Figure 5). The increase in the hydrodynamic size of the bioconjugates when compared to the AuNPs could indicate the binding of the ssDNA probes to the surface of the AuNPs [65]. In a similar study by Miao et al. [63], the average hydrodynamic size of 35.5 nm AuNPs increased to 46.8 nm upon the addition of 0.0037 μm oligonucleotides.

Although the probes used in this study had an identical number of nucleotide bases, they exhibited varying hydrodynamic sizes. This discrepancy was attributed to differences in probe orientation and conformation upon binding to the AuNPs, as reported in previous studies [58, 62, 63]. Furthermore, electrostatic interactions and steric hindrances further modulated the probe conformations, thus contributing to the observed variations in the hydrodynamic sizes [58, 63].

Using DLS, the charge of the nanoparticles was evaluated using the zeta potential parameter. This parameter is used to quantify the net surface charge of a particle in a solution and is often used as a guide to indicate the stability of nanoparticles in a solution [66, 67]. According to Carone et al. [67], stable nanoparticles have zeta potential values above +30 and below −30 mV.

In Figure 6, the unmodified/bare AuNPs exhibited a negative zeta potential value (−19.6 mV), consistent with their citrate-capped surface. Upon bioconjugation with the ssDNA probes, the surface charge became progressively less negative (i.e., −2.82 mV for *KatG*), indicating successful surface modification.

Overall, the DLS measurements revealed a narrow size distribution, indicating uniform particle dispersion and minimal aggregation. Furthermore, the average hydrodynamic diameter remained consistent across replicates, confirming colloidal stability while the zeta potential values were within the range associated with stable AuNPs in suspension, suggesting sufficient electrostatic repulsion between the AuNPs. These results validate the physicochemical integrity of the bioconjugates and support their suitability for downstream biosensing applications. Similar trends were reported by Mereuta et al. [68], where unhybridized ssDNA bound to AuNPs led to a shift in the zeta potential without promoting aggregation. These findings therefore corroborate the UV–vis and DLS results, confirming probe attachment and stable bioconjugate formation under the evaluated conditions [67–70].

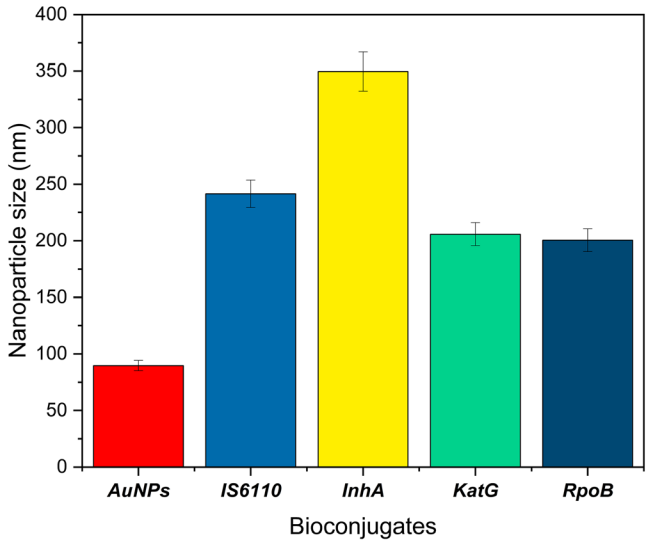

FIGURE 5 | Mean nanoparticle sizes (in nm) before and after the functionalization of the thiolated probes (error bars indicate the SEM) for each gene target (*IS6110*, *InhA*, *KatG*, and *RpoB*).

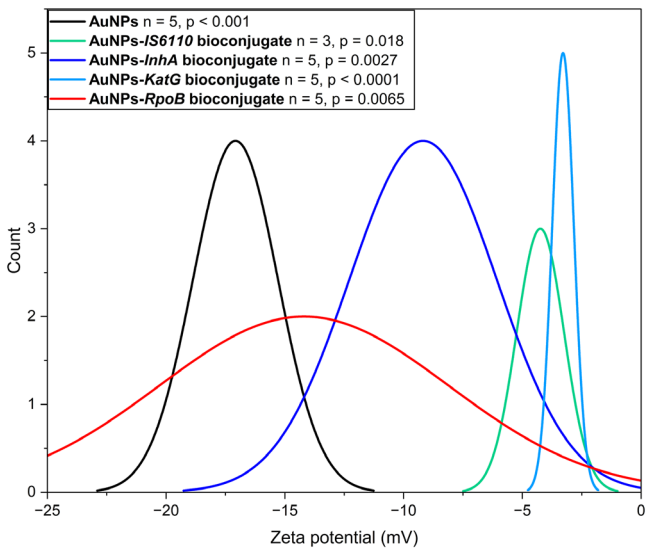

FIGURE 6 | Zeta potential values of bare AuNPs and bioconjugates corresponding to gene targets *IS6110*, *InhA*, *KatG*, and *RpoB*.

3.3 | SPR Biosensing of MDR-TB Gene Mutations

In this study, on the SPR biosensing platform, the hybridization of the capture and target molecules was recorded as analytical signals indicating the reflected intensities and angle shifts before and after DNA hybridization (Figure 7a–d).

In Figure 7a–d, the resonance angles for the references (Au only) for each gene were observed at 45.51 (*IS6110*), 45.81 (*InhA*), 45.67 (*KatG*), and 45.46 (*RpoB*) degrees. Moreover, the immobilization of each probe onto the sensor chip surface resulted in resonance angles of 46.01, 45.93, 45.81, and 45.55 degrees for gene targets *IS6110*, *InhA*, *KatG*, and *RpoB*, respectively. Subsequently, the functionalization of the targets onto the sensing surface with the probe (for each gene) resulted in positive angle shifts of 46.85 (*IS6110*), 46.77 (*InhA*), 45.84 (*KatG*), and 46.91 (*RpoB*) degrees. This observation coincides with several similar studies that attributed positive angle shifts to the hybridization of molecules on the sensing platforms [71–73].

In contrast, when the immobilized probes on the sensor surface were exposed to the non-complementary targets, negative angle shifts for all genes were noted when compared to the probe-complementary target angle shifts. The observed resonance angles were 46.33, 46.05, 45.53, and 45.85 degrees for *IS6110*, *InhA*, *KatG*, and *RpoB* genes, respectively. The addition of the non-complementary target to the probe (except for the *KatG* gene) on the SPR sensor chip surface resulted in no major angle shifts from the angle shifts noted for the immobilized probe only (Figure 7a,b,d). The observed signal variation, in several studies, was attributed to the absence of hydrogen bonding between non-complementary DNA strands, which disrupts the hybridization process and alters probe-target interactions [74–76]. This disruption is often reflected in subtle angular deviations of the capture probe, as demonstrated in studies where non-complementary sequences induced measurable shifts in probe orientation [74–76]. Moreover, such angular changes have been linked to the immobilization geometry of DNA probes on sensor surfaces, which significantly influences hybridization efficiency and signal transduction [75, 76].

In contrast, the SPR response for the *KatG* gene with the non-complementary target showed a resonance angle shift that

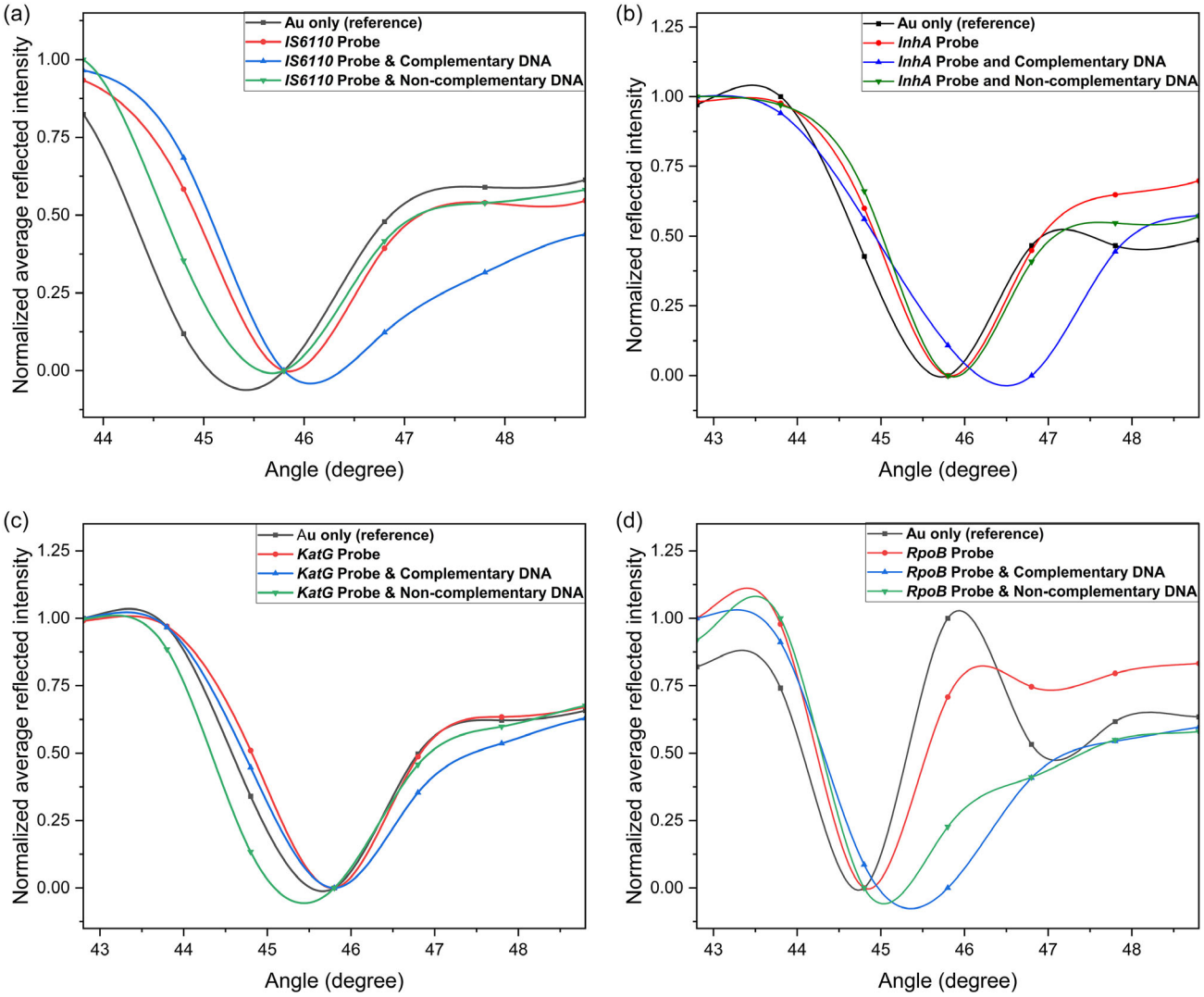

FIGURE 7 | SPR responses of the immobilized probes and the hybridization of MDR-TB targets (a) *IS6110*, (b) *InhA*, (c) *KatG*, and (d) *RpoB*. The curves represent the normalized reflected intensities and resonance angle shifts of the sequential addition of probe, complementary target, and non-complementary target to the sensor chip.

reverted to a resonance angle less than the observed resonance angle for the reference (Au only). This observation can be explained using the Maxwell–Garnett theory, which attributes an SPR blueshift (shift to the left/negative angle shift) to the biomolecules dissolving into the matrix of the biosensor chip [77].

Overall, although the SPR resonance angle shifts are small, these shifts are consistent with previous DNA hybridization studies, where single base mismatches produced measurable angular deviations due to disrupted altered probe-target dynamics [59, 75, 76, 78]. Mean resonance angles for each gene are summarized in Table 3 (Supplementary A).

The calculated corresponding repeatability percentages for each gene in three independent SPR experiments are indicated in Table 2. The repeatability values, which ranged between 98.84 and 99.59, indicated that the results obtained for each successive SPR measurement carried out under the same conditions were consistent with the observed outputs.

A Tukey's HSD test was used to examine the significant differences between the interactions of the probes with the complementary and non-complementary targets. For each gene, the Tukey's HSD test indicated significant differences between the resonance angles observed for the probes with the complementary targets and compared to the probes with the non-complementary targets. In addition, the p-values for all genes were $p < 0.001$. Levene's test for homogeneity of variances (absolute deviations) indicated no significant differences ($p > 0.05$) between the variances of the data observed for the complementary and non-complementary targets for all genes of interest.

Subsequently, the linear responses of various probe concentrations on the biosensing platform were assessed to determine the corresponding LOD and LOQ values for each gene of interest (Figure 8). The LOD and LOQ values were calculated using Equations (2) and (3).

The resonance angles measured at various probe concentrations were corrected by subtracting the reference data from the Au-coated sensor chip (Figure 8). Each gene exhibited linear responses, with slopes of 0.067 (*IS6110*), 0.040 (*InhA*), 0.055 (*KatG*), and 0.064 (*RpoB*). In addition, using Equation (2) and a reference standard deviation of 0.035, the calculated LODs were 1.72, 2.89, 2.10, and 1.81 μM/mL for *IS6110*, *InhA*, *KatG*, and *RpoB*, respectively. The corresponding LOQ values, calculated

TABLE 2 | The repeatability of the SPR measurements, based on the mean resonance angle shifts, for four genes of interest (*IS6110*, *InhA*, *KatG*, and *RpoB*).

Genes	Repeatability percentages (%; ± SEM)			
	Au only	Probe	Probe and complementary	Probe and non-complementary
IS6110	99.41 (±0.0046)	99.36 (±.0051)	99.46 (±0.0033)	99.59 (±0.0063)
InhA	99.35 (±0.0051)	99.34 (±0.0081)	99.53 (±0.0065)	99.05 (±0.0083)
KatG	98.90 (±0.0088)	98.90 (±0.0086)	98.91 (±0.0088)	99.16 (±0.0049)
RpoB	98.84 (±0.0079)	99.20 (±0.0128)	99.05 (±0.0082)	98.93 (±0.0074)

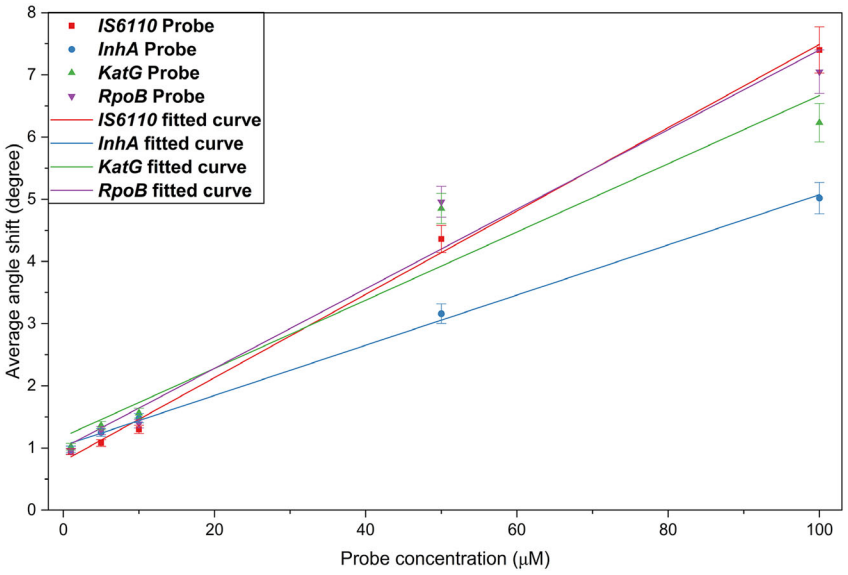

FIGURE 8 | Calibration curves of mean resonance angle shifts corresponding to different probe concentrations on the SPR sensor chip.

using Equation (3), were 5.22 (*IS6110*), 8.75 (*InhA*), 6.36 (*KatG*), and 5.47 μM/mL (*RpoB*). In contrast, current MDR-TB diagnostic assays, such as Xpert MTB/RIF, line probe assays, and nucleic acid amplification tests (NAATs), which use real-time PCR, exhibit LODs of ≈131, 10,000, and 15 CFU/mL, respectively [79]. These values correspond to estimated DNA concentrations of 0.22, 16.95, and 0.03 μM/mL, depending on DNA yield per cell.

The calculated LOD values for the SPR biosensing platform used in this study are comparable to those reported for the NAAT assays; however, while our approach shows promise for detecting MDR-TB using synthetic samples, its clinical applicability remains limited by clinical sample benchmarking and validation. To bridge this gap, future work will focus on rigorously benchmarking sensitivity and specificity using clinical samples and integrating the platform into microfluidic point-of-care devices to enable rapid, low-resource diagnostics. Additionally, multiplexing capabilities will be optimized for improved diagnostic breadth. Finally, key challenges such as biomarker complexity and variability due to multiple genetic mutations, sample processing, and instrumentation costs are potential constraints in developing a DNA-based SPR sensor for MDR-TB diagnosis. Despite these constraints, the sensor promises for a rapid diagnostic tool and drug resistance surveillance for MDR-TB.

4 | Conclusion

In this study, we demonstrated the differences in the absorption intensity of the AuNPs when bound to different concentrations of thiolated ssDNA probes using UV–vis. This method indicated that with increasing probe concentration, there was a decrease in the absorption intensity of the AuNPs. Furthermore, we used DLS to investigate the hydrodynamic size and surface charge (zeta potential) of the AuNPs before and after bioconjugation with the thiolated probes. While the hydrodynamic size of the AuNPs indicated an increase in the hydrodynamic size of the AuNPs with each bioconjugation, the surface charge of the bioconjugates exhibited zeta potential charge values that suggest reduced electrostatic stability. The UV–vis and DLS results, therefore, confirmed that the nanoparticles remained dispersed, due to steric effects from ssDNA conjugation. We further demonstrated the use of SPR in assessing the hybridization properties of capture probes and target ssDNA on the sensor surface. We highlighted the differences in the resonance angles after the immobilization of the probe, target ssDNA (complementary), and mismatched ssDNA (non-complementary). The subsequent changes in the resonance angles indicated probe immobilization onto the sensor surface and hybridization between the immobilized probe and the target ssDNA. Overall, we demonstrated the use of SPR as a label-free biosensing approach for the detection of drug-resistant TB genes.

Author Contributions

Sipho H. Chauke: conceptualization, data curation, formal analysis, investigation, methodology, software, validation, visualization, writing – original draft, writing – review and editing. **Lerato Hlekelele**: writing – review and editing, DLS data curation and methodology. **Charles Maphanga**: conceptualization, methodology, writing – review, and editing. **Mabotse Tjale**: conceptualization, methodology, writing – review, and editing. **Felix S. Dube**: writing – review and editing, supervision. **Saturnin Ombinda-Lemboumba**: conceptualization, methodology, writing – review, and editing. supervision. **Patience Mthunzi-Kufa**: funding acquisition, supervision, writing, review, and editing.

Acknowledgments

The authors acknowledge with gratitude the financial support provided by the Department of Science and Innovation (DSI), which made this research possible. We further recognize the contributions of the Council for Scientific and Industrial Research (CSIR) for access to specialized facilities and instrumentation essential to the experimental work.

Funding

The Department of Science and Innovation (DSI), the Council for Scientific and Industrial Research (CSIR), and CHIETA bursary sponsorship financially supported this work.

Conflicts of Interest

The authors declare no conflicts of interest.

Data Availability Statement

The data that support the findings of this study are available from the corresponding author upon reasonable request.

References

1. K. A. Yusoof, J. I. García, A. Schami, et al., "Tuberculosis Phenotypic and Genotypic Drug Susceptibility Testing and Immunodiagnostics: A Review," *Frontiers in Immunology* 13 (2022): 870768, https://doi.org/10.3389/fimmu.2022.870768.

2. World Health Organization, Global Tuberculosis Report 2023, 2023.

3. World Health Organization, Global Tuberculosis Report, Geneva, 2024, 2024.

4. I. Shah, V. Poojari, and H. Meshram, "Multi-Drug Resistant and Extensively-Drug Resistant Tuberculosis," *Indian Journal of Pediatrics* 87 (2020): 833.

5. K. Naidoo, R. Perumal, S. L. Ngema, L. Shunmugam, and A. M. Somboro, *Pathogens* 13 (2024): 27, https://doi.org/10.3390/pathogens13010027.

6. World Health Organization, *Implementing the WHO Stop TB Strategy: A Handbook for National Tuberculosis Control Programmes* (World Health Organization Press (WHO Press), 2008), ISBN: 978-92-4-154667-6.

7. World Health Organization, *WHO Consolidated Guidelines on Tuberculosis. Module 1, Prevention: Tuberculosis Preventive Treatment* (World Health Organization Press (WHO Press), 2020), Vol. 1, ISBN: 978-92-4-000150-3.

8. L. Nandlal, R. Perumal, and K. Naidoo, "Rapid Molecular Assays for the Diagnosis of Drug-Resistant Tuberculosis," *Infection and Drug Resistance* 15 (2022): 4971.

9. A. Rahman, M. Sahrin, S. Afrin, et al., "Comparison of Xpert MTB/RIF Assay and GenoType MTBDRplus DNA Probes for Detection of Mutations Associated with Rifampicin Resistance in Mycobacterium Tuberculosis," *PLoS One* 11 (2016) p.e0152694, https://doi.org/10.1371/journal.pone.0152694.

10. S. Tiberi, N. Utjesanovic, J. Galvin, et al., "Drug Resistant TB – Latest Developments in Epidemiology, Diagnostics and Management," *International Journal of Infectious Diseases* 124 (2022): S20.

11. G. Günther, N. Ruswa, and P. M. Keller, "Drug-Resistant Tuberculosis: Advances in Diagnosis and Management," *Current Opinion in Pulmonary Medicine* 28 (2022): 211.

12. T. N. A. Nguyen, V. A. Le Berre, A. L. Bañuls, and T. V. A. Nguyen, *Frontiers in Microbiology* 10 (2019): 794, https://doi.org/10.3389/fmicb.2019.00794.

13. Q. Liu, D. Yang, B. Qiu, et al., *Plos Neglected Tropical Diseases* 15 (2021): 1.

14. R. Mishra, P. Shukla, W. Huang, and N. Hu, "Gene Mutations in Mycobacterium Tuberculosis: Multidrug-Resistant TB as an Emerging Global Public Health Crisis," *Tuberculosis* 95 (2015): 1.

15. D. I. Ling, A. A. Zwerling, and M. Pai, "GenoType MTBDR Assays for the Diagnosis of Multidrug-Resistant Tuberculosis: A Meta-Analysis," *European Respiratory Journal* 32 (2008): 1165.

16. World Health Organization (WHO), *WHO Consolidated Guidelines on Tuberculosis. Module 3: Diagnosis - Rapid Diagnostics for Tuberculosis Detection* 3rd ed. (World Health Organization Press (WHO Press), (2024), ISBN: 978-92-4-008948-8.

17. P. Nath, A. Kabir, S. K. Doust, Z. J. Kreais, and A. Ray, *Diagnostics* 10 (2020): 841, https://doi.org/10.3390/diagnostics10100841.

18. Z. Li, L. Leustean, F. Inci, M. Zheng, U. Demirci, and S. Wang, "Plasmonic-Based Platforms for Diagnosis of Infectious Diseases at the Point-of-Care," *Biotechnology Advances* 37 (2019): 107440, https://doi.org/10.1016/j.biotechadv.2019.107440.

19. C. Wang, M. Liu, Z. Wang, S. Li, Y. Deng, and N. He, "Point-of-Care Diagnostics for Infectious Diseases: From Methods to Devices," *Nano Today* 37 (2021): 101092, https://doi.org/10.1016/j.nantod.2021.101092.

20. P. Damborský, J. Švitel, and J. Katrlík, "Optical Biosensors," *Essays in Biochemistry* 60 (2016): 91.

21. A. K. Singh, S. Mittal, M. Das, A. Saharia, and M. Tiwari, "Optical Biosensors: A Decade in Review," *Alexandria Engineering Journal* 67 (2023): 673.

22. P. Singh, "SPR Biosensors: Historical Perspectives and Current Challenges," *Sensors and Actuators. B, Chemical* 229 (2016): 110.

23. O. V. Shynkarenko and S. A. Kravchenko, "Surface Plasmon Resonance Sensors: Methods of Surface Functionalization and Sensitivity Enhancement," *Theoretical and Experimental Chemistry* 51 (2015): 273.

24. M. Puiu and C. Bala, "SPR and SPR Imaging: Recent Trends in Developing Nanodevices for Detection and Real-Time Monitoring of Biomolecular Events," *Sensors* 16 (2016): 870, https://doi.org/10.3390/s16060870.

25. H. Šípová and J. Homola, "Surface Plasmon Resonance Sensing of Nucleic Acids: A Review," *Analytica Chimica Acta* 773 (2013): 9.

26. R. Karlsson, E. Pol, and Å. Frostell, "Comparison of Surface Plasmon Resonance Binding Curves for Characterization of Protein Interactions and Analysis of Screening Data," *Analytical Biochemistry* 502 (2016): 53.

27. T. Xue, X. Cui, W. Guan, et al., "Surface Plasmon Resonance Technique for Directly Probing the Interaction of DNA and Graphene Oxide and Ultra-Sensitive Biosensing," *Biosensors & Bioelectronics* 58 (2014): 374.

28. A. Paul, C. Musetti, R. Nanjunda, and W. D. Wilson, In *Methods in Molecular Biology*, (Humana Press Inc., 2019). 63–85.

29. M. Drozd, S. Karoń, and E. Malinowska, "Recent Advancements in Receptor Layer Engineering for Applications in SPR-Based Immunodiagnostics," *Sensors* 21 (2021): 3781, https://doi.org/10.3390/s21113781.

30. Y. Huang, L. Zhang, H. Zhang, et al., "Development of a Portable SPR Sensor for Nucleic Acid Detection," *Micromachines* 11 (2020): 526, https://doi.org/10.3390/mi11050526.

31. C. V. Topor, M. Puiu, and C. Bala, "Strategies for Surface Design in Surface Plasmon Resonance (SPR) Sensing," *Biosensors* 13 (2023): 465, https://doi.org/10.3390/bios13040465.

32. D. E. P. Souto, J. Volpe, C. de C. Gonçalves, C. H. I. Ramos, and L. T. Kubota, "A Brief Review on the Strategy of Developing SPR-Based Biosensors for Application to the Diagnosis of Neglected Tropical Diseases," *Talanta* 205 (2019), https://doi.org/10.1016/j.talanta.2019.120122.

33. E. Ferrari, "Gold Nanoparticle-Based Plasmonic Biosensors," *Biosensors* 13 (2023): 411, https://doi.org/10.3390/bios13030411.

34. A. Karnwal, R. S. Kumar Sachan, I. Devgon, et al., "Gold Nanoparticles in Nanobiotechnology: From Synthesis to Biosensing Applications," *ACS Omega* 9 (2024): 29966.

35. T. Mocan, C. T. Matea, T. Pop, et al., "Development of Nanoparticle-Based Optical Sensors for Pathogenic Bacterial Detection," *Journal of Nanobiotechnology* 15 (2017), https://doi.org/10.1186/s12951-017-0260-y.

36. B. A. Prabowo, A. Purwidyantri, B. Liu, H. C. Lai, and K. C. Liu, "Gold Nanoparticle-Assisted Plasmonic Enhancement for DNA Detection on a Graphene-Based Portable Surface Plasmon Resonance Sensor," *Nanotechnology* 32 (2021): 095503, https://doi.org/10.1088/1361-6528/abcd62.

37. I. Choi and Y. Choi, "Plasmonic Nanosensors: Review and Prospect," *IEEE Journal on Selected Topics in Quantum Electronics* 18 (2012): 1110.

38. S. Mourdikoudis, R. M. Pallares, and N. T. K. Thanh, "Characterization Techniques for Nanoparticles: Comparison and Complementarity upon Studying Nanoparticle Properties," *Nanoscale* 10 (2018): 12871.

39. M. Zając, J. Kotyńska, G. Zambrowski, et al., "Exposure to Polystyrene Nanoparticles Leads to Changes in the Zeta Potential of Bacterial Cells," *Scientific Reports* 13 (2023): 9552, https://doi.org/10.1038/s41598-023-36603-5.

40. A. W. Russ, *A Brief Introduction to Traditional Bioconjugate Chemistry*, (Wiley-VCH Verlag GmbH & Co. KGaA, 2017). ISBN: 978-3-527-33436-0 (Print); 978-3-527-68345-1 (Online). https://doi.org/10.1002/9783527683451.ch1.

41. S. B. Nimse, K. Song, M. D. Sonawane, D. R. Sayyed, and T. Kim, "Immobilization Techniques for Microarray: Challenges and Applications," *Sensors* 14 (2014): 22208.

42. M. Pirzada and Z. Altintas, "Recent Progress in Optical Sensors for Biomedical Diagnostics," *Micromachines* 11 (2020): 356, https://doi.org/10.3390/MI11040356.

43. O. Tokel, U. H. Yildiz, F. Inci, et al., "Portable Microfluidic Integrated Plasmonic Platform for Pathogen Detection," *Scientific Reports* 5 (2015): 9152, https://doi.org/10.1038/srep09152.

44. R. Wang, S. Tombelli, M. Minunni, M. M. Spiriti, and M. Mascini, "Immobilisation of DNA Probes for the Development of SPR-Based Sensing," *Biosensors & Bioelectronics* 20 (2004): 967.

45. B. A. Prabowo, A. Alom, M. K. Secario, et al., In *Procedia Engineering* (Elsevier Ltd., 2016). 541–545.

46. M. Trzaskowski, A. Napiórkowska, E. Augustynowicz-Kopeć, and T. Ciach, "Detection of Tuberculosis in Patients with the use of Portable SPR Device," *Sensors and Actuators B, Chemical* 260 (2018): 786.

47. A. M. Shrivastav, U. Cvelbar, and I. Abdulhalim, "A Comprehensive Review on Plasmonic-Based Biosensors Used in Viral Diagnostics," *Communications Biology* 4 (2021): 70, https://doi.org/10.1038/s42003-020-01615-8.

48. B. A. Prabowo, Y. F. Chang, H. C. Lai, et al., "Rapid Screening of Mycobacterium Tuberculosis Complex (MTBC) in Clinical Samples by a Modular Portable Biosensor," *Sensors and Actuators B, Chemical* 254 (2018): 742.

49. M. Matsishin, A. Rachkov, A. Errachid, S. Dzyadevych, and A. Soldatkin, "Development of Impedimetric DNA Biosensor for

Selective Detection and Discrimination of Oligonucleotide Sequences of the rpoB Gene of Mycobacterium Tuberculosis," *Sensors and Actuators. B, Chemical* 222 (2016): 1152.

50. A. Rachkov, S. Patskovsky, A. Soldatkin, and M. Meunier, "Discrimination of Single Base Mismatched Oligonucleotides Related to the *rpoB* Gene of *Mycobacterium Tuberculosis* Using a Surface Plasmon Resonance Biosensor," *Biotechnology and Applied Biochemistry* 60 (2013): 453.

51. S. H. Chauke, S. Ombinda-Lemboumba, F. Dube, and P. Mthunzi-Kufa, "*Optical Biosensing of Multidrug-resistant Tuberculosis (TB) Genes*," Proc. SPIE 12840, Optical Interactions with Tissue and Cells XXXV, 128400B (12 March 2024), https://doi.org/10.1117/12.3002279.

52. A. Shrivastava and V. Gupta, "Methods for the Determination of Limit of Detection and Limit of Quantitation of the Analytical Methods," *Chronicles of Young Scientists* 2 (2011): 21.

53. A. Minhas-Khan, M. Ghafar-Zadeh, T. Shaffaf, et al., "UV-Vis Spectrophotometric Analysis of DNA Retrieval for DNA Storage Applications," *Actuators* 10 (2021): 246, https://doi.org/10.3390/act10100246.

54. B. McCarte, O. T. Yeung, A. J. Speakman, A. Elfick, and K. E. Dunn, "Using Ultraviolet Absorption Spectroscopy to Study Nanoswitches Based on Non-Canonical DNA Structures," *Biochemistry and Biophysics Reports* 31 (2022): 101293, https://doi.org/10.1016/j.bbrep.2022.101293.

55. S. Ngernpimai, T. Puangmali, A. Kopwitthaya, P. Tippayawat, A. Chompoosor, and S. Teerasong, "Enhanced Stability of Gold Nanoparticles with Thioalkylated Carboxyl-Terminated Ligands for Applications in Biosensing," *Acs Applied Nano Materials* 7 (2024): 13124.

56. M. Giersig and P. Mulvaney, "*Preparation of Ordered Colloid Monolayers by Electrophoretic Deposition*," (American chemical society (ACS), 1993): 3408–3413, https://doi.org/10.1021/la00036a014.

57. K. Mahato, S. Nagpal, M. A. Shah, et al., "Gold Nanoparticle Surface Engineering Strategies and Their Applications in Biomedicine and Diagnostics," *3 Biotech* 9 (2019): 57, https://doi.org/10.1007/s13205-019-1577-z.

58. M. Cárdenas, J. Barauskas, K. Schullén, J. L. Brennan, M. Brust, and T. Nylander, *Langmuir* 22 (2006): 3294.

59. Q. Zhang, X. N. Zou, and L. Q. Chu, "Surface Plasmon Resonance Studies of the Hybridization Behavior of DNA-Modified Gold Nanoparticles with Surface-Attached DNA Probes," *Plasmonics* 13 (2018): 903.

60. H. Zhang, X. Li, F. He, M. Zhao, and L. Ling, "Turn-Off Colorimetric Sensor for Sequence-Specific Recognition of Single-Stranded DNA Based upon Y-Shaped DNA Structure," *Scientific Reports* 8 (2018): 295–305, https://doi.org/10.1038/s41598-018-30529-z.

61. R. Singhal, D. Kabiraj, P. K. Kulriya, J. C. Pivin, R. Chandra, and D. K. Avasthi, "Blue-Shifted SPR of Au Nanoparticles with Ordering of Carbon by Dense Ionization and Thermal Treatment," *Plasmonics* 8 (2013): 295.

62. N. C. Allen, R. Chauhan, P. J. Bates, and M. G. O'Toole, "Optimization of Tumor Targeting Gold Nanoparticles for Glioblastoma Applications," *Nanomaterials* 12 (2022): 3869, https://doi.org/10.3390/nano12213869.

63. X. M. Miao, C. Xiong, W. W. Wang, L. S. Ling, and X. T. Shuai, "Dynamic-Light-Scattering-Based Sequence-Specific Recognition of Double-Stranded DNA with Oligonucleotide-Functionalized Gold Nanoparticles," *Chemistry - A European Journal* 17 (2011): 11230.

64. G. A. Morris, J. Castile, A. Smith, G. G. Adams, and S. E. Harding, "The Effect of Prolonged Storage at Different Temperatures on the Particle Size Distribution of Tripolyphosphate (TPP) – Chitosan Nanoparticles," *Carbohydrate Polymers* 84 (2011): 1430.

65. Q. Dai, X. Liu, J. Coutts, L. Austin, and Q. Huo, "A One-Step Highly Sensitive Method for DNA Detection Using Dynamic Light Scattering," *Journal of the American Chemical Society* 130 (2008): 8138.

66. W. Wang, X. Ding, Q. Xu, J. Wang, L. Wang, and X. Lou, "Zeta-Potential Data Reliability of Gold Nanoparticle Biomolecular Conjugates and Its Application in Sensitive Quantification of Surface Absorbed Protein," *Colloids and Surfaces B, Biointerfaces* 148 (2016): 541.

67. A. Carone, S. Emilsson, P. Mariani, A. Désert, and S. Parola, "Gold Nanoparticle Shape Dependence of Colloidal Stability Domains," *Nanoscale Advances* 5 (2023): 2017.

68. L. Mereuta, A. Asandei, I. S. Dragomir, et al., "Sequence-Specific Detection of Single-Stranded DNA with a Gold Nanoparticle-Protein Nanopore Approach," *Scientific Reports* 10 (2020), https://doi.org/10.1038/s41598-020-68258-x.

69. S. Bhattacharjee, "DLS and Zeta Potential–what They are and What They are Not?" *Journal of Controlled Release* 235 (2016): 337.

70. L. Hlekelele, K. Setshedi, V. Mandiwana, et al., "Carboxy-PEG-Thiol Functionalized Gold Nanoparticle Conjugates for the Detection of SARS-CoV-2: Detection Tools and Analytical Method Development," *Journal of Virological Methods* 330 (2024): 115028, https://doi.org/10.1016/j.jviromet.2024.115028.

71. S. De, R. Kundu, A. Ghorai, R. P. Mandal, and U. Ghosh, "Green Synthesis of Gold Nanoparticles for Staining Human Cervical Cancer Cells and DNA Binding Assay," *Journal of Photochemistry and Photobiology. B, Biology* 140 (2014): 130.

72. L. Soares, A. Csáki, J. Jatschka, et al., "Localized Surface Plasmon Resonance (LSPR) Biosensing Using Gold Nanotriangles: Detection of DNA Hybridization Events at Room Temperature," *The Analyst* 139 (2014): 4964.

73. F. Zheng, Z. Chen, J. Li, et al., "A Highly Sensitive CRISPR-Empowered Surface Plasmon Resonance Sensor for Diagnosis of Inherited Diseases with Femtomolar-Level Real-Time Quantification," *Advanced Science* 9 (2022): 2105231, https://doi.org/10.1002/advs.202105231.

74. J. I. A. Rashid and N. A. Yusof, "The Strategies of DNA Immobilization and Hybridization Detection Mechanism in the Construction of Electrochemical DNA Sensor: A Review," *Sensing and Bio-Sensing Research* 16 (2017): 19.

75. T. Sasaki, K. Masuda, Z. Zhang, et al., "Quantitative Evaluation of DNA Probe Density by Electrochemical Surface Plasmon Resonance Measurement" *Sensors and Materials* 34 (2022): 927.

76. T. Haque and H. K. Rouf, "DNA Hybridization Detection Using Graphene-MoSe2–Ag Heterostructure-Based Surface Plasmon Resonance Biosensor," *Applied Physics. A, Materials Science & Processing* 127 (2021): 759, https://doi.org/10.1007/s00339-021-04888-w.

77. U. Kreibig, and M. Vollmer, *Optical Properties of Metal Clusters* 13 (1995): 532.

78. A. Pathak, M. Meena, and S. Tripathi, "Performance Analysis of Graphene-Coated GaAs SPR Sensor for Detection of DNA Hybridization," *Physics of the Solid State* 63 (2021): 453.

79. A. M. I. Saktiawati, A. Vasiliu, F. Saluzzo, and O. W. Akkerman, "Strategies to Enhance Diagnostic Capabilities for the New Drug-Resistant Tuberculosis (DR-TB) Drugs," *Pathogens* 13 (2024): 1045, https://doi.org/10.3390/pathogens13121045.

Supporting Information

Additional supporting information can be found online in the Supporting Information section. **Supporting Table S1:** A summary of the mean resonance angle values obtained for each gene of interest detected using the SPR setup.